



OPEN

The synergistic interference effect of silica nanoparticles concentration and the wavelength of ELISA on the colorimetric assay of cell toxicity

Fariba Abbasi¹, Hassan Hashemi¹, Mohammad Reza Samaei^{1✉}, Amir SavarDashtaki², Aboolfazl Azhdarpoor¹ & Mohammad Javad Fallahi³

The 3-(4,5-dimethylthiazol-2-yl)-2,5-diphenyltetrazolium bromide (MTT) assay is the most common method for the determination of cell toxicity, but some factors limit the sensitivity of this method, such as pH. Less attention had been paid to the interference effect of optical and plasmonic properties of SiO₂ nanoparticles (NPs) in the wavelength range assigned to MTT. This study investigated the synergistic interference effect of SiO₂ NPs and wavelength on MTT assay for the first time. The examined variables included the type of SiO₂ NPs concentrations (1, 10, and 100 mM) and different wavelengths (470, 490, 520, and 570 nm). The results showed that optical density (OD) increased ($p < 0.05$) when wavelength and the concentration of crystalline SiO₂ NPs increased. So, the maximum OD at 10 and 100 mM were attributed to crystalline SiO₂ NPs ($p < 0.05$) due to the functional group, whereas it was related to amorphous at 1 mM ($p > 0.05$). According to polynomial regression modeling (PRM), the maximum interference effect was predicted at crystalline SiO₂ NPs and wavelength > 550 nm. Besides, the synergistic effects of SiO₂ NPs, wavelength, and concentration of NPs had been a good fitting with first-order PRM. Thus, the concentration of SiO₂ NPs had a confounder factor in colorimetric for MTT assay. The best artificial neural network (ANN) structure was related to the 3:7:1 network ($R_{\text{all}} = 0.936$, $\text{MSE} = 0.0006$, $\text{MAPE} = 0.063$). The correlation between the actual and predicted data was 0.88. As SiO₂ NPs presence is an interfering factor in MTT assay concerning wavelength, it is suggested wavelength use with minimum confounding effect for MTT assay.

3-(4,5-Dimethylthiazol-2-yl)-2,5-diphenyltetrazolium bromide (MTT) is one of the most common methods for the determination of cell proliferation and cellular toxicity assay. MTT is an attractive method compare to others, such as methylene blue^{1,2}. It is widely used to determine the toxicity effects of various drugs and nanoparticles in industry and medicine. This method is based on the colorimetric assay, that tetrazolium salt is reduced to formazan by donor electron. This reaction can be due to the presence of Nicotinamide adenine dinucleotide (NADH) produced by the mitochondria of living cells, as well as superoxide³⁻⁶. The approximate level of living cells is estimated based on the purple dye intensity⁷. Although this is a simple and repeatable method⁸, it has limitations such as nonspecific adsorption, relatively poor sensitivity, and low surface to volume ratio. These limitations in some cases can challenge, and invalidate the evaluation process basis⁹. Previous studies have shown that certain conditions, such as antioxidants, change of pH range, reducing agents, temperature variation, and the type of solvents, are the disruption factors on regeneration formazan and MTT test^{6,10-12}. On the other hand, some studies have suggested a reaction between nanoparticles and these efficient factors in MTT. In Popescu's study, the MTT-formazan complex was formed on TiO₂ NPs¹³. In this condition, about 14% of false viability in the MTT was related to the TiO₂-MTT reaction¹⁴. Moreover, Fe³⁺ are acted as a strong reaction inhibitor that is

¹Department of Environmental Health Engineering, School of Health, Shiraz University of Medical Sciences, Shiraz, Iran. ²Department of Medical Biotechnology, School of Advanced Medical Sciences and Technologies, Shiraz University of Medical Sciences, Shiraz, Iran. ³Department of Internal Medicine, School of Medicine, Shiraz University of Medical Sciences, Shiraz, Iran. ✉email: mrsamaei@sums.ac.ir

Variables	Unit	The range of variables
Wavelength	nm	470, 490, 520, and 570
Calcination temperature	°C	70, 350, 600, 800 and 1000
Concentration of SiO ₂ NPs	mM	1, 10, and 100

Table 1. The investigated variables.

interfered with the MTT assay¹³. Other structures, such as graphene, be efficient in light-absorbing and transmitting during the colorimetric process¹⁵. Thus, the same effects may be due to the presence of other substances and NPs. SiO₂ nanoparticles (NPs) are stable NPs¹⁶, that are widely used in industry, medicine, and pharmaceuticals. Besides, its crystalline structures are an environmental pollutant that can oxidize the human organs¹⁷. Commonly MTT assay is used to determine the effectiveness or toxicity of SiO₂ NPs on invitro. However, there has been less attention paid to the interference effects of SiO₂ NPs on MTT qualitatively and quantitatively because they have been introduced as a surface reactivity agent that can produce radicals such as OH[•]. Therefore, it can involve in redox reaction and amplify the tetrazolium reduction^{18,19}. Moreover, formazan is a pH-sensitive dye that also binds to the surface of SiO₂ NPs²⁰. Finally, the silica matrix is encapsulated during the polymerization process of color molecules²¹. On the other hand, silica has certain optical properties that can affect colorimetric assay, as light transmission and reflection²². These differences and properties can be changed during the different wavelengths that become more significant with nanoparticle crystallization. The amounts of light transmission from silica have gradually increased at a wavelength < 500 nm, whereas the maximum absorption was at 520 nm^{23–25}. According to logarithmic slope in light transmission and the maximum capability of SiO₂ NPs for adsorption in 400–600 nm range, as maximum adsorption of formazan at 570 nm⁶. It is expected that the co-presence of silica and formazan can disrupt the actual results of MTT because MTT is evaluated in the same wavelength range. These interference effects have been less studied, and the relationships between them properly have not been defined. Most events in vitro and real scale have nonlinear relationships that require the use of nonlinear models. Due to this necessity and with the hypothesis of the interfering factor of these nanoparticles, it is necessary to study the nonlinear relationship to predict the MTT reading rate by ELISA reader. Among nonlinear methods, the artificial neural network (ANN) is more accurate in predicts of events. Besides, MTT is based on colorimetric assay and optical properties attributed to the wavelength performance²⁶. Moreover, the optical and plasmonic properties of silica resonance increase in the wavelength range of MTT as increasing light absorption with time increases^{27,28}. This study aimed to investigate the interference effect of SiO₂ NPs, their concentrations on MTT assay, and its modeling using regression and ANN model.

Materials and methods

Synthesis of SiO₂ nano particles. In this study, SiO₂ NPs were synthesized using the Stober method²⁹. This method is one of the well-known sol–gel methods for synthesizing nanoparticles. According to this method, Tetraethyl orthosilicate (TEOS, Merck Germany ≥ 99.0%) was used as the raw material for SiO₂ NPs synthesis. Ethanol (Merck Germany 100.0%) and ammonia (Merck Germany 25.0%) were used as solvent and catalyst, respectively. Deionized water (Merck Germany) was also used for dilution. The synthesis was performed in an ultrasonic bath, after aging, the obtained gel was washed with ethanol and water. Then the product was dried at 24 °C for 24 h. Nanoparticles were also crystallized using thermal methods at different temperatures (350, 600, 800, and 1000 °C). X-ray powder diffraction (XRD) graph was used to investigate the crystallization degree of NPs. Then field emission scanning electron microscopy (FESEM) and energy dispersive spectroscopy (EDS) results were interpreted to determine the size and purity percentage of NPs. Also, NPs distribution in the solution was determined by dynamic light scattering (DLS)³⁰.

Experiment design. This study was a full factorial design. The investigated variables was included the wavelength used for the enzyme-linked immunosorbent assay (ELISA) reader, the calcination temperature (CT) of the NPs, and the concentration of NPs in the cell culture media. The total number of experimental conditions were assessed was 60 with triplicate. The range of all variables examined is shown in Table 1.

Experimental analysis. To determine the SiO₂ NPs interference effect on the MTT assay, the SiO₂ NPs solutions were prepared at 1, 10, and 100 mM. Later they were transferred into media containing MTT salt. Therefore, MTT assay conditions were simulated, and the prepared solution was incubated at 37 °C for four hr. Finally, the purple color obtained from the MTT assay was read by the ELISA. For determination of the wavelength effect, optical density (OD) was determined at 470, 490, 520, and 570 nm.

Artificial neural network modelling. ANN is one of the modeling methods to determine the nonlinear relationship between variables which has several input variables, hidden, and output layers. In this model, the number of neurons in each hidden layer has a significant effect on the response. In the present study, using MATLAB 2018, the feed-forward backpropagation algorithm (Levenberg–Marquardt algorithm) was used for modeling. Initially, the network was trained with OD obtained at different wavelengths (470, 490, 520, and 570 nm) obtained from the ELISA. In this model, 70, 15, and 15% of the data were used for training, validation, and testing, respectively. After training, the amount of error validation was monitored, and after increasing the error with a specific repetition, training stops. The best ANN structure was determined based on mean square

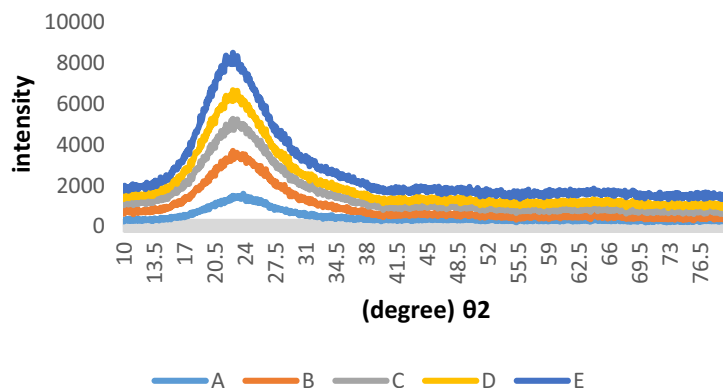


Figure 1. XRD patterns of SiO₂ NPs (A) dried at 70 °C, (B) calcinated at 350 °C, (C) calcinated at 600 °C, (D) calcinated at 800 °C, and (E) calcinated at 1000 °C.

error (MSE), mean absolute percentage error (MAPE), and correlation coefficient (R) in the hidden layer, which was used to predict the interfering effect of SiO₂ NPs on OD obtained from MTT assay. A hidden layer is located between the input and output of the algorithm. It is applied for weighting to inputs to provide the output. The performance of the hidden layer base on nonlinear function and the efficiency of ANN associated with the layer significantly. In this study, the number of neurons in the hidden layer was determined based on the most comprehensive equation in environmental toxicology, such as nanoparticles toxicology. It is expressed in both Eqs. (1) and (2):

$$\frac{2(i + o)}{3} < n < i(i + o) - 1, \quad (1)$$

$$0.5i - 2 < n < 2i + 2, \quad (2)$$

i is the number of inputs, o is the the number of outputs and n is the number of hidden layer neuron.

Statistical analysis. OD at 470, 490, 520, and 570 nm were determined using descriptive statistics. It was compared at each stage using a one-way analysis of variance (ANOVA) test at different temperatures. The correlation between OD and the variables was performed by Spearman correlation. The significant difference was adjusted to 0.05. The interference effect of nanoparticles Modeling was performed using linear, cubic, quadric, surface response, and polynomial regression models. Then the best regression model was selected based on R², adjusted-R², MAPE, and root-mean-square error (RMSE). Statistical analysis, tests, and modeling have been performed in MATLAB 2018.

Ethics approval and consent to participate. All ethical aspects of this study were approved by Shiraz University of medical science' Ethics Committee (IR.SUMS.REC.1398.1226).

Consent for publication. Not applicable.

Results and discussion

The characteristic of SiO₂ NPs. In this study, the crystallization process of SiO₂ NPs was investigated during CT between 70 and 1000 °C, as shown in Fig. 1.

The XRD peak in all nanoparticles was 22–24 °C (Fig. 1). They were confirmed that the SiO₂ NPs were converted to crystal lattices during the increase of CT. In previous studies, the XRD peak for SiO₂ NPs in amorphous and crystal was 14°–21° and 26°–27°, respectively^{31–33}. Besides, crystallization increased with increasing calcination temperature up to 1000 °C because amorphous SiO₂ NPs were formed at low temperatures (70–150 °C)³⁴. Instead, as crystallization increases (from A to E), regular lattices were created. Subsequently, the NPs surface reactivity was reduced, and strong bonds were formed between silica and oxygen.

SiO₂ NPs have been identified in the range of 400–1400 cm⁻¹ in the Fourier-transform infrared spectroscopy (FTIR) spectra³⁵. Some of the functional groups in FTIR spectra of investigated SiO₂ NPs are expressed in Table 2.

According to Table 2, the maximum light transmittance in all nanoparticles was in the range of 1070–1085 cm⁻¹. This range was determined the bond between Si–O and the functional groups coupled to this bond^{36–38}. So, the presence of the Si–OCH₃ bond was confirmed in E NPs. This bond is an active functional group that reacts to more substance. In addition, there was a spectrum between 616 and 797 cm⁻¹ in D and E NPs that identified as depicted siloxane. The triple bond in depicted siloxane is an effective factor in the reactivity of SiO₂ NPs³⁹. Thus, increasing the calcination temperature increased the crystallinity of SiO₂ NPs, but more investigation was essential to determine the regeneration of formazan in MTT assay and its interference-effect.

SiO ₂ NPs	Bonds
A	Si–O, Si–OH, Si–O–Si, Si–Cl
B	Si–O, Si–OH, Si–O–Si, Si–Cl, O–H
C	Si–O, Si–O–Si, Si–Cl, Si–H
D	Si–O, Si–OH, Si–O–Si, Si–Cl, O–H, hydroxyl group, ≡Si–O–Si≡
E	Si–O, Si–OH, Si–O–Si, Si–Cl, O–H, hydroxyl group, ≡Si–O–Si≡

Table 2. The functional group of SiO₂ NPs (A) amorphous, (B) calcinated at 350 °C, (C) calcinated at 600 °C, (D) calcinated at 800 °C, and (E) calcinated at 1000 °C.

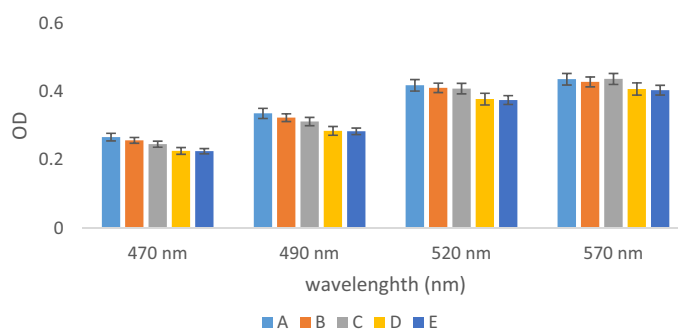


Figure 2. The ratio of OD of SiO₂ NPs compare to control sample during different wavelength (A) amorphous, (B) calcinated at 350 °C, (C) calcinated at 600 °C, (D) calcinated at 800 °C, and (E) calcinated at 1000 °C.

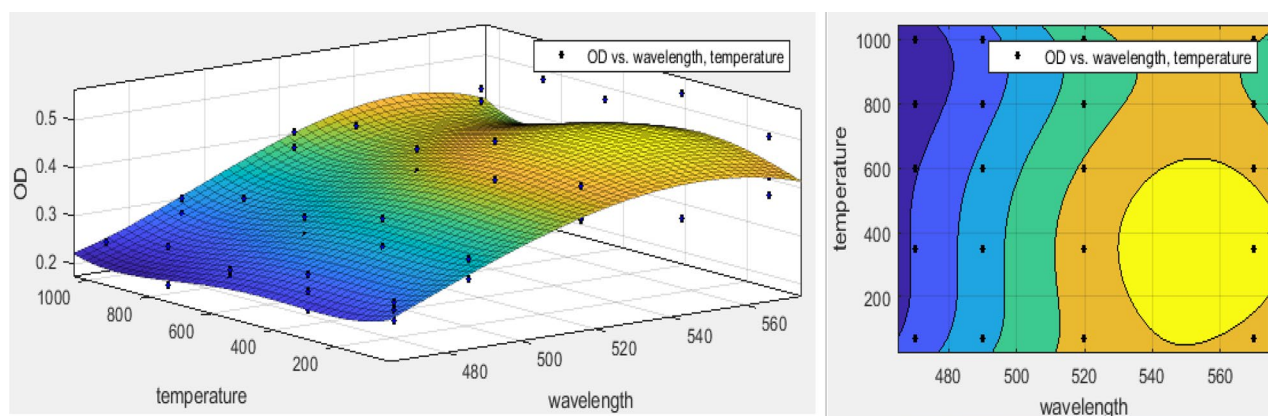


Figure 3. The synergistic effect of wavelength and calcination temperature of SiO₂ NPs using polynomial regression model.

Interference effect of SiO₂ NPs on OD during the CT at different wavelengths. The OD percent due to SiO₂ NPs (A, B, C, D, and E) at four wavelengths of 470, 490, 520, and 570 nm is shown in Fig. 2.

According to Fig. 2, the OD was increased as wavelengths increasing. So, maximum OD was determined at the wavelength of 570 nm ($p < 0.0001$) because the refractive index decreases with increasing wavelength. This index showed the speed of light passing through a substance⁴⁰. Light transmission and maximum absorption amount significantly were dependent on the alloy crystal and its size²³. It was reported that wavelength increasing in 400–600 nm, the amount of light transmission increased from 20 to 70%²². Despite it was increased exponentially and was became almost constant after 600 nm⁴¹. In this study, the OD was decreased when the calcination temperature was increased in all wavelengths ($p < 0.005$). The results of Matysiak et al. study showed that during the crystallization of SiO₂ NPs, the absorption increased at a wavelength > 325 nm. Consequently, the light transmittance decreased because the content of Si increased in crystal nanoparticles²⁶. Polynomial regression modeling showed that the maximum interference effect of wavelength and calcination temperature of SiO₂ NPs had been related to the temperature range of in the range of 70–600 °C as well as wavelength 550 nm (Fig. 3). The equation of this relationship is expressed in Eq. (3).

The interference of parameters	SSE	R-square	Adjusted R-square	RMSE	Effective weight	MAPE	Fitted model
Concentration and temperature	0.61	0.94	0.94	0.1	Non	0.4	Cubic
Wavelength and temperature	0.1375	0.7	0.62	0.05	Concentration	0.1	Linear
Concentration and wavelength	0.037	0.921	0.9137	0.02606	Non	0.48	Quadratic

Table 3. The performance of polynomial regression model for prediction of interference effect of variables.

$$f(x, y) = 16.18 - 0.1x + 0.03y + 0.0002x^2 - 0.0002xy + 0.000006y^2 - 0.000002x^3 + 0.000003x^2y - 8 \times 10^{-9}xy^2 - 4.6 \times 10^{-9}y^3 - 2.3 \times 10^{-10}x^3y - 1.9 \times 10^{-12}x^2y^2 + 5.8 \times 10^{-12}xy^3 + 9.1 \times 10^{-13}y^4. \quad (3)$$

That

X is the wavelength (nm) and y is the temperature (°C).

According to Eq. (3) and Table 3, R-square > 0.9 and MAPE < 10%. Moreover, there was no difference between R-squared and adjusted R-square. Therefore, all of them confirmed that the cubic polynomial regression model had excellent forecasting for the prediction of the interference effect of wavelength and temperature on OD in MTT assay⁴².

According to Fig. 3, although the light can pass from the media containing SiO₂ NPs at higher wavelengths^{43–45} and were functional groups on D and E NPs (Table 2). It may involve in oxidation–reduction reaction and even bonded to formazan. Hence, the presence of SiO₂ NPs was a confounder factor in the colorimetric of MTT assay, especially during higher wavelengths (Fig. 3). Based on these results, it is best to use an MTT assay for the determination of crystalline nanoparticles toxicity that was calcinated at high temperatures. It was suggested that the wavelengths < 500 nm used to determine the toxicity of SiO₂ NPs.

The effect of SiO₂ NPs concentration on OD. The OD attributed to concentrations of 1, 10, and 100 mM of SiO₂ NPs are shown in Fig. 4.

As shown in the 1 mM concentration, OD increased with increasing wavelength (Fig. 4a). The OD of A, B, C, D, and E were detected between 0.27–0.5 (p < 0.0001), 0.29–0.54, 0.26–0.49, 0.19–0.33, and 0.27–0.499. Hence, the highest coefficient of variation (CV) was related to all concentrations of B NPs (p < 0.0001), but with increasing calcination temperature, CV has decreased (p < 0.05). Nevertheless, the maximum and minimum ODs were determined in the media containing B and D NPs (p < 0.05) which, were calcinated at 350 °C and 600 °C, respectively.

According to Fig. 4b (concentrations = 10 mM), OD level of A, B, C, D and E NPs were 0.24–0.42 (p > 0.05), 0.257–0.45, 0.23–0.39, 0.21–0.38, and 0.247–0.443 (p < 0.05), respectively. OD was increased during the increasing of wavelengths (p < 0.05). At all studied wavelengths, there was an insignificance difference between the minimum and maximum OD in E and B NPs (p > 0.05).

At a concentration = 100 mM, by wavelength increasing, the OD has increased (Fig. 4c). The OD of A, B, C, D, and E were 0.286–0.382 (p < 0.0001), 0.22–0.29, 0.22–0.29, 0.21–0.34, and 0.22–0.42 (p < 0.0001), respectively. The maximum and minimum ODs were attributed to E and D NPs (p < 0.05), respectively. Also, the highest CV was estimated in E NPs (p < 0.0001). The Pearson test showed an insignificant correlation between CT and OD (p < 0.05). In low concentrations, increasing calcination temperature be effective in increasing OD (p < 0.04). While, in high concentrations, a similar trend has not been observed (p > 0.05). Also, concerning the effect of NPs concentration, the polynomial regression models have been shown a significant effect related to the simultaneous influence of CT and wavelength with 95% confidence bounds (R-square: 0.94 and RMSE: 0.1) as well as the weighting with the concentration of SiO₂ NPs. Therefore, the weighting of this model with concentration was predicted well by PRM (first-order equation). although R-square > 0.6 shown that it might be satisfactory in some applications, the insignificant difference between R-squared and adjusted R-square (< 0.01) as MAPE = 10 confirmed the capability of this model (Table 3)⁴². The equation of this relationship and its three-dimensional diagram are shown in Eq. (4) and Fig. 5, respectively.

$$f(x, y) = 0.0015x - 0.00004y - 0.4428, \quad (4)$$

X is the wavelength (nm) and y is the calcination temperature (°C).

Based on Fig. 6, there was no significant difference between OD of 1, 10, and 100 mM (p > 0.05). With the increasing wavelength of the ELISA, significant differences were observed (p < 0.05). The regression model was shown the synergistic effects of all variables of concentration, wavelength, and incubation temperature. Remarkably, it was found that the concentration of silica nanoparticles was a confounder factor in colorimetric used in MTT assay because the concentration of silica has been identified as an interfering factor in the absorption and transmission of light²⁶. The maximum interference effect of SiO₂ NPs was at wavelengths = 560 nm and in amorphous nanoparticles (Fig. 5). This result was increased with increasing the SiO₂ NPs concentration. Each of these variables can be attributed to another as the calcination temperature of SiO₂ NPs and the ELISA wavelength. Therefore, the simultaneous effect of the wavelength, concentration, and calcination temperature investigated by regression models. The regression modeling of simultaneous effects of wavelength and NPs concentrations using the surface response is shown in Fig. 6.

Moreover, the equation of this interaction was expressed in Eq. (5).

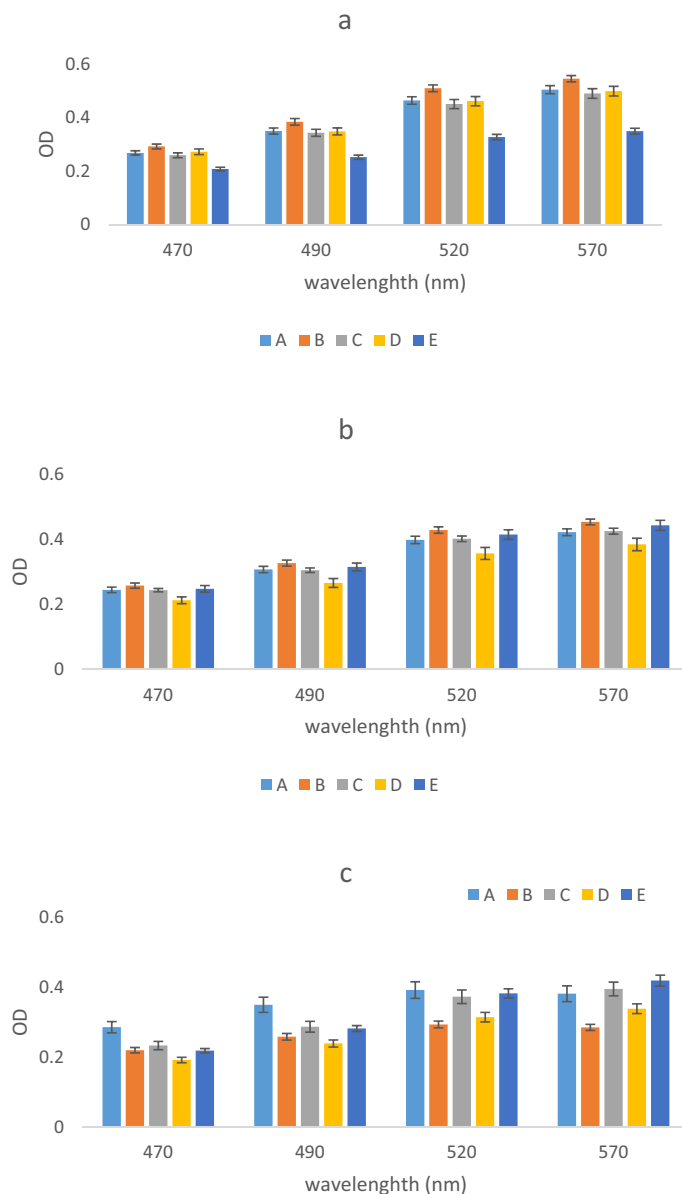


Figure 4. The OD ratio of SiO₂ NPs compare to control sample during different wavelength (a) 1 mM, (b) 10 mM and (c) 100 mM. (A) amorphous, (B) calcinated at 350 °C, (C) calcinated at 600 °C, (D) calcinated at 800 °C, and (E) calcinated at 1000 °C.

$$f(x, y) = 0.03x - 0.0026y - 0.00002x^2 - 0.000005xy + 0.000046y^2 - 7.73, \quad (5)$$

X is the wavelength (nm) and y is the concentration of SiO₂ NPs (mM).

As shown in Fig. 6, the interfering effects of SiO₂ NPs were increased at concentrations lesser and higher than 20 mM 100 mM, respectively. Moreover, the peak of interference effect was predicted at lower concentrations (R-square: 0.921, MAPE = 0.48, and RMSE: 0.02606) without a variables selection as a weight of the model. Concerning Table 3, R-square > 0.9, the insignificant difference between R-squared and adjusted R-square (< 0.01) as well as MAPE = 20–50% (MAPE = 48%). This model had good forecasting for the prediction of this interference effect⁴². No such interference effects have been observed during wavelength < 480 nm. It can be concluded that the selection of wavelength for MTT assay has been related to the concentration of SiO₂ NPs.

The modelling of interference of SiO₂ on OD using ANN. According to Fig. 3, the simultaneous effect of CT and wavelength has been fitted with polynomial regression models (R-square: 0.7 and RMSE: 0.05). The R² > 0.6 may be satisfactory in some applications therefore, the regression model couldn't be the most effective model for the prediction of some relationship between both parameters. Other studies used machine learning methods to predict cell toxicity as deep learning, random forests, k-nearest neighbors, and support vector machines⁴⁶. But the use of ANN has been introduced as a useful, reliable, cheap, and fast tool for predicting the

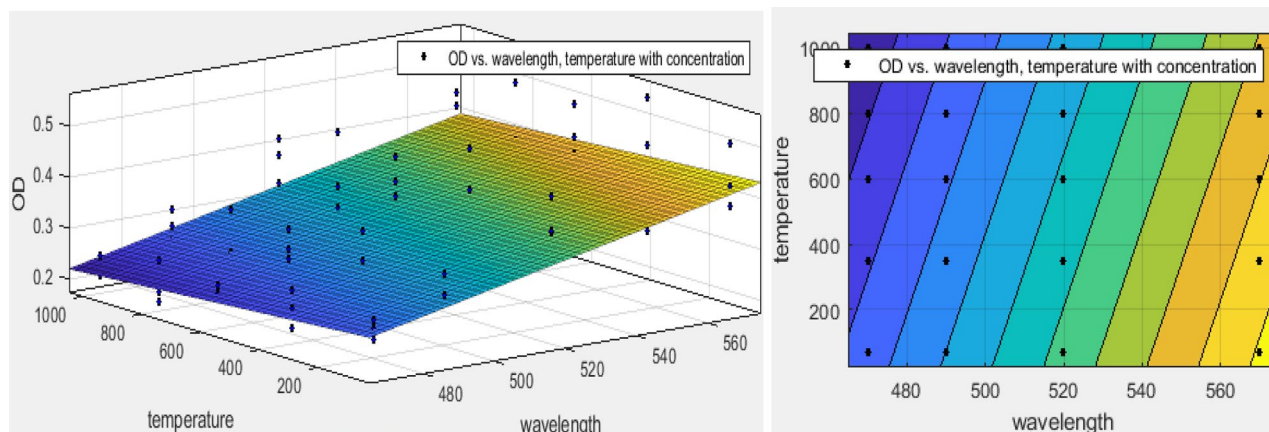


Figure 5. The synergistic effect of wavelength, calcination temperature and concentration of SiO₂ NPs using polynomial regression model.

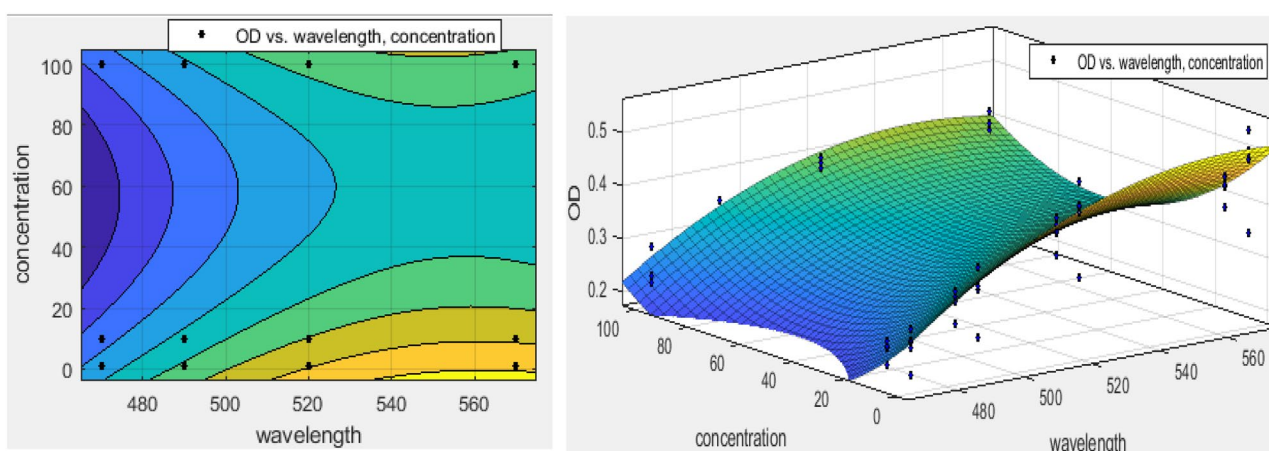


Figure 6. The synergistic effect of wavelength and concentration of SiO₂ NPs using polynomial regression model.

Structure of ANN	R (all)	R (test)	R (training)	R (validation)	MSE	MAPE	Optimum epochs	Stop validation	Gradient range
3:8:1	0.902	0.95	0.889	0.918	0.0011	0.074	4	10	10 ⁻² –10 ⁻⁴ (0.0008)
3:7:1	0.936	0.934	0.929	0.975	0.0006	0.063	2	8	10 ⁻³ –10 ⁻⁴ (0.0001)
3:6:1	0.932	0.958	0.928	0.957	0.00099	0.071	8	14	10 ⁻² –10 ⁻⁴ (0.0007)
3:5:1	0.923	0.956	0.914	0.965	0.0013	0.086	1	6	10 ⁻² –10 ⁻⁴ (0.0004)
3:4:1	0.908	0.877	0.920	0.802	0.002	0.23	5	11	10 ⁻² –10 ⁻⁴ (0.0003)

Table 4. The results of the number of neurons in hidden layer (4–8 neuron).

non-linear relationship between variables such as OD in MTT⁴⁷. The Levenberg–Marquardt (LM) algorithm was used to determine the best network structure for weight and bias. Because these algorithms have the a higher predictive capacity for the toxicity of nanoparticles in biology media compare to others as deep neural networks^{48,49}. According to this method, the number of neurons the in hidden layer based on Eqs. (1) and (2) were 2.6 to 11 and – 0.5 to 8, respectively. Then the intersection of both intervals (3–8 neurons) was selected for ANN training. Based on the number of input and output variables, the number of neurons in the hidden layer=3–8 was used to predict wavelength transmission using ANN. The best of them according to Table 4 was related to 7 neurons in the hidden layer. After all, it had the highest correlation coefficient ($R_{all}=0.936$,

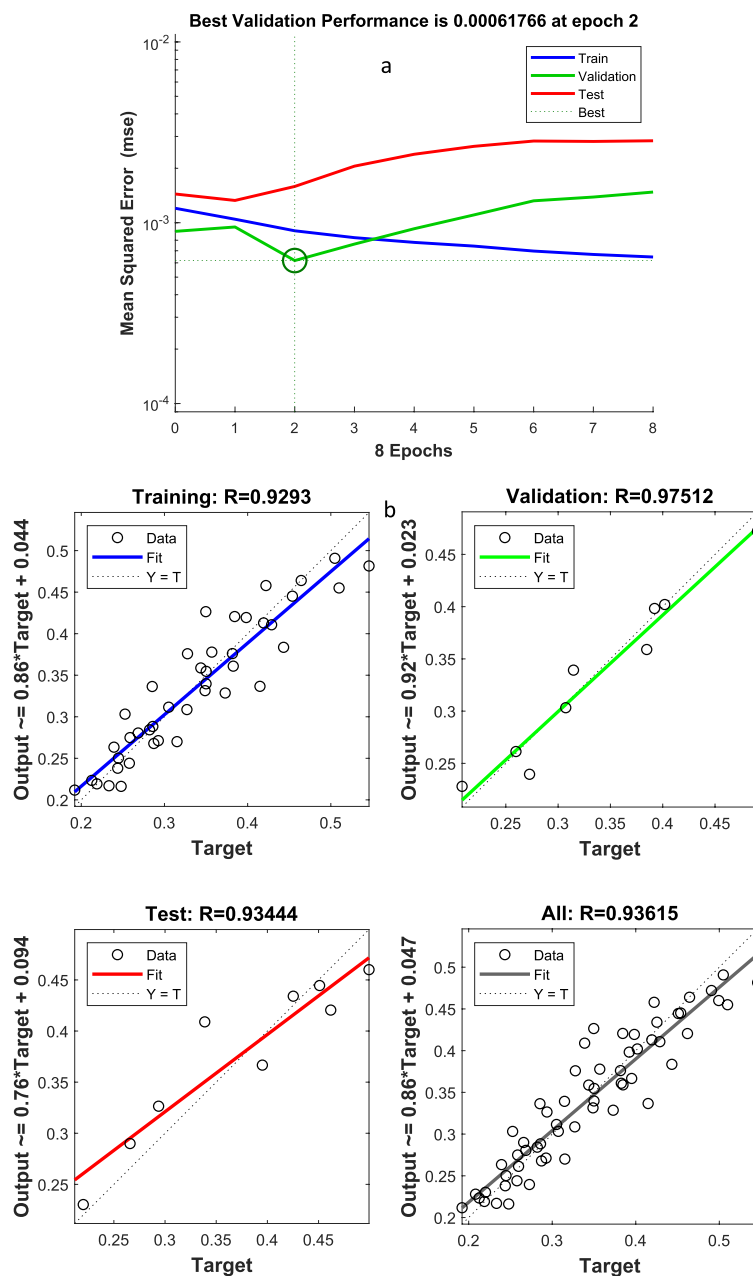


Figure 7. The MSE and regression of the best model for prediction of wavelength transmission.

$R_{\text{training}} = 0.929$, $R_{\text{validation}} = 0.975$ and $R_{\text{test}} = 0.934$ and the lowest MSE = 0.0006 as well as MAPE = 0.063 because the MAPE is less sensitive to outliers. Moreover, the gradient of this structure was lower than others (Gradient = 0.0001). On another word, the prediction of ANN was more than PRM (see Tables 3 and 4). Besides, Fig. 7 also shows the structure of the best predictive model and the relationship between input and output by the hidden layer. Because the trend of validation and test error was similar, and there was no overfitting before the epoch of 2. But the validation error increased for seven iterations significantly that training is stopped based on the stop algorithm. Moreover, the regression coefficient in Fig. 7b showed the correlation in the test dataset = 0.934 and all test = 0.937.

The prediction using ANN compared to the experimental value is shown in Table S1. The maximum and minimum transmission wavelengths in real samples were 1 mM and 100 mM, respectively, which were 350 °C and 800 °C (runs of 16 and 45). In the ANN results, the minimum light transmission at a concentration of 100 mM was 470 nm and was related to calcinated nanoparticles at a temperature of 800 °C. The maximum prediction results by ANN were for amorphous nanoparticles, 1 mM concentration, and 570 nm wavelength, respectively. Thus, the neural network well can predict the interference effect of nanoparticles on OD. It has a limit to predict the amount of OD at higher wavelengths. In Fig. 8, the correlation between the values predicted by the ANN model versus the actual value obtained from the laboratory data was 0.88, which shows an acceptable correlation

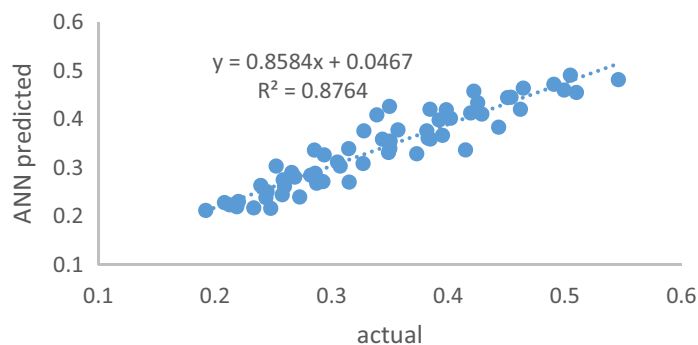


Figure 8. The wavelength transmission for the actual laboratory results and the predicted by ANN model.

between the network output and the transmission wavelength. Therefore, the ANN had a suitable ability to predict the wavelength transmission of media containing different amorphous types and crystalline nanoparticles with different concentrations. But in addition to these results, further studies on light absorption and reflection and its prediction using other nonlinear models are suggested.

Sensitivity analysis. In this study, the effect of some parameters on MTT assay was investigated and modeled by ANN. But the determination of the most effective of these parameters is an essential step to designing further studies. Hence, identifying and focusing on effective parameters can decrease the actual interference and errors in the laboratory test. Therefore, we use the sensitivity analysis that corresponds to statistical techniques focused on determining how the variations of the M input variables of a mathematical model influence the response value⁵⁰. According to enter linear regression model, the beta coefficient was used to predict the effect of the studied variables. This correlation was 0.038, -0.429 , and -0.241 for calcination temperature of silica nanoparticles, nanoparticle concentration, and the wavelength of ELISA-reader, respectively. Among the studied variables, the effective factor was nanoparticles concentration, which was negatively related to OD amount. This correlation was less for decreasing wavelength and increasing the calcination temperature of nanoparticles. Consequently, the calcination of nanoparticles was the most important interference effect on OD of ELISA-reader.

Conclusion and suggestion

This study investigated the interference effect of different concentrations of SiO₂ NPs on MTT assay during different wavelengths and modeled by ANN. According to results, the crystallization rate of SiO₂ NPs and the existence of reactive functional group as Si-OCH₃ and depicted siloxane bonds has increased with increasing CT up to 1000 °C. The OD level increased with wavelength increasing and decreased the CT. So, the maximum OD was determined at the wavelength = 570 nm ($p < 0.0001$). Based on PRM, the maximum interference effect of wavelength and CT of NPs were attributed to the temperature range of 70–600 °C and wavelength 550 nm. Moreover, OD was increased when increased the wavelength at the concentration of 1 mM. Based on Pearson correlation, there was a significant difference between OD with an increasing wavelength of the samples. The simultaneous effect of CT, wavelength, and concentration with 95% confidence bounds have been good fitting with the first-order RPM. Therefore, the co-presence of CT, wavelength, and concentration were an interference factor on colorimetric in MTT assay especially at a wavelength = 560 nm and in amorphous nanoparticles. As the SiO₂ concentration NPs increased, the synergistic effects of all three variables increased significantly. The best structure of the ANN using the LM algorithm was related to 3:7:1 with all datasets (0.936) and test dataset (0.934) as MSE = 0.0006. The correlation between the values predicted by the ANN model versus the actual value obtained from the laboratory data was 0.88, which indicates an acceptable correlation between the network output and the amount of OD. Sensitivity analysis using enter linear regression model was showed the beta coefficient was 0.038, -0.429 , and -0.241 for calcination temperature of SiO₂ NPs, nanoparticle concentration, and the wavelength of ELISA-reader, respectively. Thus, among the studied variables, the most effective factor was the concentration of nanoparticles (Supplementary Information).

Concerning our results and the effect of SiO₂ NPs concentration and structure as well as the wavelength of MTT on OD, it is suggested to perform an MTT assay based on the control sample (i.e. the same concentration of SiO₂ NPs in media without cell). So, the OD of control samples should decrease from case samples. Moreover, the concentration of SiO₂ NPs should be selected based on the lowest interference effect. Although this study was investigated the effect of several parameters on the toxicity assay (MTT) for the first time, there was some limitation for this study. Therefore, it was suggested that the effect of cell media and some characteristics of SiO₂ NPs such as transmittance and reflectance of them as optical parameters especially absorption coefficient and optical constants determine during the MTT assay. Moreover, the prediction of them was modeled by other models.

Data availability

The supporting data are available from the corresponding author on reasonable request.

Received: 1 September 2020; Accepted: 9 June 2021

Published online: 23 July 2021

References

- Selvakumaran, J. & Jell, G. *A Guide to Basic Cell Culture and Applications in Biomaterials and Tissue Engineering* (CRC Press, 2005).
- Luis, C., Castaño-Guerrero, Y., Soares, R. & Sales, G. Avoiding the interference of doxorubicin with MTT measurements on the MCF-7 breast cancer cell line. *Methods Protoc.* **2**, 29 (2019).
- Volk, P. D. & Moreland, J. G. Methods in enzymology. *Endosome Signal. Part B.* **535**, 430 (2014).
- Riss T. L. *et al.* Cell Viability Assays. In: (eds Markossian, S. *et al.*). *Assay Guidance Manual*. Bethesda (MD): Eli Lilly & Company and the National Center for Advancing Translational Sciences; 2004. <https://www.ncbi.nlm.nih.gov/books/NBK144065/>. (2016).
- Emanet, M., Şen, Ö. & Çulha, M. Evaluation of boron nitride nanotubes and hexagonal boron nitrides as nanocarriers for cancer drugs. *Nanomedicine (Lond)*. **12**(7), 797–810. <https://doi.org/10.2217/nnm-2016-0322>. (2017).
- Sittampalam, G. S. *et al.* *Assay Guidance Manual* (Eli Lilly Company & Company and the National Center for Advancing Translational Sciences, 2019).
- Winikoff, S. E. & Lotez, M. T. *Cytotoxic Assay Measuring Immunity* (Elsevier, 2005).
- Thiha, A. & Ibrahim, F. A colorimetric enzyme-linked immunosorbent assay (ELISA) detection platform for a point-of-care dengue detection system on a lab-on-compact-disc. *Sensors* **15**, 11431–11441 (2015).
- Lai, X., Gao, G., Watanabe, J., Liu, H. & Shen, H. Hydrophilic polyelectrolyte multilayers improve the ELISA system: Antibody enrichment and blocking free. *Polymers* **9**, 51 (2017).
- Kitamura, M. & Hiramatsu, N. The unfolded protein response and cellular stress, part B. *Methods Enzymol.* **490**, 30–38 (2011).
- Prasad, S. *et al.* Near UV–Visible electronic absorption originating from charged amino acids in a monomeric protein. *Chem. Sci.* **8**, 5416–5433 (2017).
- Gasque, C. K. S., Al-Ahj, L. P., Oliveira, R. C. & Magalhães, C. A. Cell density and solvent are critical parameters affecting formazan evaluation in MTT assay. *Braz. Arch. Biol. Technol.* **57**(3), 381–385 (2014).
- Popescu, T., Lupu, A. R., Raditoiu, V. & Purcar, V. on the photocatalytic reduction of MTT tetrazolium salt on the surface of TiO₂ nanoparticles: Formazan production kinetics and mechanism. *J. Colloid Interface Sci.* **457**, 108–120 (2015).
- Lupu, A. R. & Popescu, T. The noncellular reduction of MTT tetrazolium salt by TiO₂ nanoparticles and its implications for cytotoxicity assay. *Toxicol. In Vitro* **27**(5), 1445–1450 (2014).
- Jiao, G. *et al.* Limitations of MTT and CCK-8 assay for evaluation of graphene cytotoxicity. *RSC Adv.* **5**, 53240–53244 (2015).
- Vasceanu, G. M. & Holban, A. M. Nanostructures for cancer therapy: From targeting to selective toxicology. In *Nanostructures for Cancer Therapy* (Elsevier, 2017).
- Zare Naghadehi, M., Sereshki, F. & Mohammadi, F. Pathological study of the prevalence of silicosis among coal miners in Iran: A case history. *Atmos. Environ.* **83**, 1–5 (2014).
- Basu, B. & Mandal, B. Chapter 9 - Sustainable Synthesis of Benzimidazoles, Quinoxalines, and Congeners. book title: *Green Synthetic Approaches for Biologically Relevant Heterocycles*. Boston. Elsevier. pp. 209–256. (2015).
- Entezari, M. *et al.* Is there a relationship between homes' radon gas of MS and non-MS individuals, and the patients' paraclinical magnetic resonance imaging and visually evoked potentials in Yazd-Iran?. *Environ. Sci. Pollut. Res.* **28**, 1–8 (2020).
- Lian, Y. & Wang, X.-D. Nanomaterials for intracellular pH sensing and imaging. In *Novel Nanomaterials for Biomedical, Environmental and Energy Applications* (Elsevier, 2019).
- Kang, H. & Tan, W. Optical biosensors. 2 edn, (ed. Frances Ligler-Chris Taitt). page 712. **eBook ISBN: 9780080564944** (2008).
- Zhang, C. *et al.* Third-order optical nonlinearity of Na₂O–B₂O₃–SiO₂ glass doped with lead nanoparticles prepared by sol–gel method. *J. Alloy. Compd.* **602**, 221–227 (2014).
- Sakthisabarimoorathi, A., Britto Dhas, S. A. & Jose, M. Study on optical nonlinearity of Au@SiO₂ composite nanoparticles towards photonic applications. *Mater. Chem. Phys.* **240**, 122154 (2020).
- Reinhard, D. K. *et al.* SiO₂ antireflection layers for single-crystal diamond. *Diam. Relat. Mater.* **25**, 84–86 (2012).
- Li, Y. *et al.* Synthesis and growth mechanism of oriented amorphous SiO₂ nanowires. *Mater. Sci. Semicond. Process.* **15**, 428–431 (2012).
- Matysiaka, W. & Tański, T. Analysis of the morphology, structure and optical properties of SiO₂ nanowires obtained by the electrospinning method. *Mater. Today Proc.* **7**, 382–388 (2019).
- Stolzenburg, H., Peretzki, P., Wang, N., Seibt, M. & Ihlemann, J. Implantation of plasmonic nanoparticles in SiO₂ by pulsed laser irradiation of gold films on SiO_x-coated fused silica and subsequent thermal annealing. *Appl. Surf. Sci.* **374**, 138–142 (2016).
- Hossain, A., Ikeda, Y., Hara, T. & Nagasaki, Y. Novel biocompatible nanoreactor for silica/gold hybrid nanoparticles preparation. *Colloids Surf. B* **102**, 778–782 (2013).
- Fernandes, R. S., Raimundo, I. M. Jr. & Pimentel, M. F. Revising the synthesis of Stöber silica nanoparticles: A multivariate assessment study on the effects of reaction parameters on the particle size. *Colloids Surf. A* **577**, 1–7 (2019).
- Abbasi, F. *et al.* The toxicity of SiO₂ NPs on cell proliferation and cellular uptake of human lung fibroblastic cell line during the variation of calcination temperature and its modeling by artificial neural network. *J. Environ. Health Sci. Engin.* **19**, 985–995. (2021).
- Fuchs, I., Aluma, Y., Ilan, M. & Mastai, Y. Induced crystallization of amorphous biosilica to cristobalite by silicatein. *J. Phys. Chem. B* **118**(8), 2104–2111 (2014).
- Sukhanov Ravani, A. *et al.* Dependence of nanoparticle toxicity on their physical and chemical properties. *Nanoscale Res. Lett.* **13**(1), 44 (2018).
- Muljani, S., Wahyudi, B. & Sumada, K. Potassium silicate foliar fertilizer grade from geothermal sludge and pyrophyllite. *MATEC Web Conf.* **58**, 01021 (2016).
- Waseem, M. *et al.* Synthesis and characterization of silica by sol–gel method. *J. Pak. Mater. Soc.* **3**, 19 (2009).
- Abadi, M. H. S., Verlag, G., Delbari, A., Fakoor, Z. & Baedi, J. Effects of annealing temperature on infrared spectra of SiO₂ extracted from rice husk. *J. Ceram. Sci. Technol.* **5**(4), 8 (2014).
- Goh, S., Shiau, L. L., Bin Mohammad, M. S. & Tan, C. S. Highly compact linear variable filter in the mid infrared region for acetone level monitoring. *IEEE Sens. J.* **99**, 1–10 (2019).
- Launer, P. J., & Arkles, B. (2013). *Infrared Analysis of Organosilicon Compounds: Spectra-Structure Relationships*. In *Silicon Compounds: Silanes and Silicones* (eds Arkles, B. & Larson, G.) (pp. 175–178). Morrisville, PA, USA: Gelest Inc. <https://doi.org/10.5281/zenodo.3696063>.
- Nariyal, R. K., Kothari, P. & Bisht, B. FTIR measurements of SiO₂ glass by sol–gel technique. *Chem. Sci. Trans.* **3**(3), 1064–1066 (2014).
- Nayak, P. P. & Nandi, S. A. K. Comparative assessment of chemical treatments on extraction potential of commercial grade silica from rice husk. *Eng. Rep.* **1**, 212035 (2019).
- Jiang, D., Jia, H. & Lu, H. Calculation for the optical parameters of the Sn-doped SiO₂ thin films by fitting the entire transmitted spectrum. *Optik* **124**, 102–106 (2013).
- Nagel, H., Metz, A. & Hezel, R. Porous SiO₂ films prepared by remote plasma-enhanced chemical vapour deposition: a novel antireflection coating technology for photovoltaic modules. *Sol. Energy Mater. Sol. Cells* **65**, 71–77 (2001).
- Ostertagová, E. Modelling using polynomial regression. *Proc. Eng.* **48**, 500–506 (2012).

43. Yang, H., Yao, X., Wang, X., Gu, X. & Wang, F. Visible room-temperature photoluminescence of Ge-doped SiO₂ glasses fabricated by a sol-gel process. *Opt. Mater.* **29**, 631–635 (2007).
44. Wang, J., Li, X., Luo, L., Zhang, S. & Lu, R. Core-shell BaMoO₄@SiO₂ nanospheres: Preparation, characterization, and optical properties. *Ceram. Int.* **39**, 9293–9298 (2013).
45. Boonpichayapha, T. *et al.* A study of thickness dependence omnidirectional anti-reflection SiO₂ nanorod array fabricated by oblique angle deposition. *Mater. Today Proc.* **4**, 6037–6042 (2017).
46. Wu, Y. & Wang, G. Machine learning based toxicity prediction: from chemical structural description to transcriptome analysis. *Int. J. Mol. Sci.* **19**(8), 2358 (2018).
47. Azizi, E., Abbasi, F., Baghapour, M. A., Shirdareh, M. R. & Shoostarian, M. R. 4-Chlorophenol removal by air lift packed bed bioreactor and its modeling by kinetics and numerical model (artificial neural network). *Sci. Rep.* **11**(1), 1–10 (2021).
48. Wang, J., Wang, G., Sun, Y. & Liu, C. Importance of the volume fraction and particle density of Ag nanoparticles to the coupling process of relief-type Ag/SiO₂ nanocomposite grating coupler. *Opt. Mater.* **98**, 109483 (2019).
49. Choi, J.-S., Ha, M. K., Trinh, T. X., Yoon, T. H. & Byun, H.-G. Towards a generalized toxicity prediction model for oxide nanomaterials using integrated data from different sources. *Sci. Rep.* **8**(1), 1–10 (2018).
50. Pichery, C. Sensitivity analysis. In *Encyclopedia of Toxicology*, 3rd edn. (ed Wexler, P.) Oxford, Academic Press. pp. 236–237 (2014).

Acknowledgements

This project was financially supported by Shiraz University of Medical Sciences, PhD thesis of Fariba Abbasi (No. 18387).

Author contributions

F.A. participated in the design of study, performing experimental, data collection and analysis and write the article. M.R.S. participated the design of study and the main edit of article. H.H., A.A. and M.J.F. participated in the design of study. A.S.D. participated in the design of study and data collection.

Funding

Shiraz University of medical science.

Competing interests

The authors declare no competing interests.

Additional information

Supplementary Information The online version contains supplementary material available at <https://doi.org/10.1038/s41598-021-92419-1>.

Correspondence and requests for materials should be addressed to M.R.S.

Reprints and permissions information is available at www.nature.com/reprints.

Publisher's note Springer Nature remains neutral with regard to jurisdictional claims in published maps and institutional affiliations.



Open Access This article is licensed under a Creative Commons Attribution 4.0 International License, which permits use, sharing, adaptation, distribution and reproduction in any medium or format, as long as you give appropriate credit to the original author(s) and the source, provide a link to the Creative Commons licence, and indicate if changes were made. The images or other third party material in this article are included in the article's Creative Commons licence, unless indicated otherwise in a credit line to the material. If material is not included in the article's Creative Commons licence and your intended use is not permitted by statutory regulation or exceeds the permitted use, you will need to obtain permission directly from the copyright holder. To view a copy of this licence, visit <http://creativecommons.org/licenses/by/4.0/>.

© The Author(s) 2021